Published in final edited form as:
Biochemistry. 2006 October 31; 45(43): 13054–13063. doi:10.1021/bi060591r.

Multiple steps determine the overall rate of the reduction of 5α-dihydrotestosterone catalyzed by human type 3 3α-hydroxysteroid dehydrogenase (AKR1C2): Implications for the Elimination of Androgens

Yi Jin and **Trevor M. Penning***
Department of Pharmacology, University of Pennsylvania School of Medicine, Philadelphia, PA 19104, U.S.A., Email: penning@pharm.med.upenn.edu

Abstract

Human type 3 3α-Hydroxysteroid dehydrogenase, or Aldo-Keto Reductase (AKR) 1C2, eliminates the androgen signal in human prostate by reducing 5α-dihydrotesterone (DHT, potent androgen) to form 3α-andostanediol (inactive androgen), thereby depriving the androgen receptor of its ligand. The k_{cat} for the NADPH-dependent reduction of DHT catalyzed AKR1C2 is 0.033 s^{-1}. We employed transient kinetics and kinetic isotope effects to dissect the contribution of discrete steps to this low k_{cat} value. Stopped-flow experiments to measure the formation of the AKR1C2·NADP(H) binary complex indicated that two slow isomerization events occur to yield a tight complex. A small primary deuterium isotope effect on k_{cat} (1.5) and a slightly larger effect on k_{cat}/K_m (2.1) were observed in the steady state. In the transient state, the maximum rate constant for single turnover of DHT (k_{trans}) was determined to be 0.11 s^{-1} for the NADPH-dependent reaction, which was about 4 fold greater than the corresponding k_{cat}. k_{trans} was significantly reduced when NADPD was substituted for NADPH, resulting in an apparent $^{D}k_{trans}$ of 3.5. Thus the effects of isotopic substitution on the hydride transfer step were masked by slow events that follow or precede the chemical transformation. Transient multiple turnover reactions generated curvilinear reaction traces, consistent with the product formation and release occurring at comparable rates. Global fitting analysis of the transient kinetic data enabled the estimate of the rate constants for the 3-step cofactor binding/release model and for the minimal ordered bi-bi turnover mechanism. Results were consistent with a kinetic mechanism in which a series of slow events, including the chemical step (0.12 s^{-1}), the release of the steroid product (0.081 s^{-1}), and the release of the cofactor product (0.21 s^{-1}), combine to yield the overall observed low turnover number.

Cytosolic hydroxysteroid dehydrogenases (HSDs), which catalyze the NADPH dependent reduction of ketosteroids to hydroxysteroids, are members of the aldo-keto reductase (AKR) superfamily 1C subfamily (1–3). By interconverting potent steroid hormones with their cognate inactive metabolites, AKR1C enzymes can regulate the occupancy of hormone receptors in

Address all correspondence to: Dr. Trevor M. Penning, Department of Pharmacology, University of Pennsylvania School of Medicine, 3620 Hamilton Walk, Philadelphia, PA 19104-6084, Phone: 215-898-9445, FAX: 215-573-2236; Email: penning@pharm.med.upenn.edu.

[1]Abbreviations and trivial names: HSD, hydroxysteroid dehydrogenase; AKR, aldo-keto reductase; AKR1C2, human type 3 3α-HSD/bile acid binding protein; DHT, 5α-dihydrotestosterone or 17β-hydroxy-5α-androstan-3-one; Diol, 3α-androstanediol or 5α-androstane-3α,17β-diol; AKR1C9, rat liver 3α-HSD; AKR1B1, human aldose reductase; AKR2B5, yeast xylose reductase; KIE, kinetic isotope effect; 5R2, type 2 5α-reductase.

[2]The nomenclature for the aldo-keto reductase superfamily was recommended by the 8th International Symposium on Enzymology & Molecular Biology of Carbonyl Metabolism, Deadwood, SD, June 29-July 3, 1996. (Also visit www.med.upenn.edu/akr)

target tissues (4–6). Four human isoforms are known to exist (AKR1C1-AKR1C4) and share higher than 87% sequence identity. Due to their distinct steroid substrate preference and tissue distribution, each individual AKR1C isoform can regulate the metabolism of different hormones. For example, the 20-ketosteroid reductase activity of AKR1C1 eliminates progesterone, the 3-ketoreductase activity of AKR1C2 eliminates 5α-dihydrotestosterone (DHT), and the 17-ketosteroid reductase activity of AKR1C3 generates the potent hormones testosterone and 17β-estradiol (6–9).

AKR1C2 is also commonly known as the human type 3 3α-HSD and bile acid binding protein. It is expressed in many tissues, including lung, liver, prostate, mammary gland, and brain (7). In steroid target tissues, such as the prostate, AKR1C2 converts DHT selectively to 3α-androstanediol (Diol) (10) (Figure 1). DHT is the most potent natural androgen known, with an affinity of 10^{-11} M for the androgen receptor. DHT activates the androgen receptor to promote embryonic and pubertal external virilization (i.e. development of male external genitalia, urethra, and prostate, and growth of facial and body hair, etc.) (11–12). High levels of DHT are implicated in diseases such as benign prostatic hyperplasia and prostate cancer. By contrast, Diol is an inactive androgen with a low affinity for the androgen receptor (K_d = 10^{-6} M). Therefore, the consequence of the reaction catalyzed by AKR1C2 is the elimination of the androgen signal in the target tissue.

The crystal structures of several AKR1Cs including those of AKR1C2 have now been solved (13–17). A number of common features have been noted including the overall structure, the cofactor binding site and the active site. AKR superfamily members have a characteristic $(\alpha/\beta)_8$ or TIM-barrel structural motif (18). The reactive center is formed by the nicotinamide ring of the cofactor and the conserved catalytic tetrad of Tyr55, Lys84, His117, and Asp50. Positions of the cofactor and catalytic tetrad in the known AKR1C structures are highly conserved. In contrast, strong variation was noticed within the structure of the steroid binding site.

AKR1C2 catalyzes an ordered bi-bi sequential mechanism (19). The macroscopic events in the minimal mechanism are outlined in Scheme 1. For the reduction of DHT, the mechanism comprises (1) binding of NADPH (rate constants defined as k_{Ab} and k_{Ar}), (2) binding of DHT (rate constants defined as k_{Bb} and k_{Br}); (3) hydride transfer (rate constants defined as k_{red} and k_{oxi}); (4) release of Diol (rate constants defined as k_{Pr} and k_{Pb}); and (5) release of $NADP^+$ (rate constants defined as k_{Qr} and k_{Qb}).

Given the structural similarity among members of the superfamily, it is not surprising that this kinetic mechanism appears to apply to all reactions catalyzed by AKR enzymes (19–22). However, previous studies have shown that different macroscopic events are responsible for the determination of the overall rate of AKR catalysis (23–25). The release of the second product, as defined by k_{Qr} in step 5, was shown to be completely or partially rate-determining for the xylose reduction catalyzed by human aldose reductase (AKR1B1) (23) and a yeast xylose reductase (AKR2B5) (24), respectively. In contrast, when the 3-keto reduction of DHT catalyzed by the rat 3α-HSD (AKR1C9) was followed, the appearance of steady state kinetic isotope effects (KIE) and the lack of burst kinetics under multiple turnover conditions indicated that the chemistry step (k_{red} of step 3) was the major contributor to rate determination (25). AKR1C9 is closely related to AKR1C2 in sequence (76% sequence homology) and in function. AKR1C9 catalyzes the strict stereospecific reduction of 3-ketosteroids to yield 3α-hydroxysteroids, while the human AKR1C enzymes including AKR1C2 are more promiscuous and can have different positional and stereochemical preference depending on the steroid substrates. In the case of DHT, both AKR1C9 and AKR1C2 catalyze the formation of Diol, however, with large differences in k_{cat} and k_{cat}/K_m (26,27). Most interestingly, the k_{cat} for the AKR1C2 catalyzed DHT reduction is 10-fold less than the k_{cat} for AKR1C9, suggesting that

either the two enzymes have the same rate limiting steps that occur at significantly different rates or that different events determine the overall k_{cat} for the two enzymes.

In this study, AKR1C2 is chosen as a representative human AKR1C enzyme. To understand the kinetic behavior of AKR1C2 and how this impacts the elimination of the androgen signal, we have investigated the contribution of discrete steps in the AKR1C2 catalyzed reduction of DHT using KIE and transient kinetic experiments. We have established microscopic rate constants for the individual steps in the minimal kinetic mechanism employing global simulation analysis of the pre-steady-state data. We find that multiple slow steps contribute to the overall decrease in k_{cat} observed for the reduction of DHT catalyzed by AKR1C2.

EXPERIMENTAL PROCEDURES

Materials

Recombinant AKR1C2 was over-expressed in *E. coli* C41(DE3) host cells transformed with the pET-16b AKR1C2 expression vector, and purified to homogeneity by successive chromatography as described previously (28,29). Purity of the enzymes was verified by SDS-polyacrylamide gel electrophoresis, and protein concentration was determined by the Bradford method (30). The final specific activity of AKR1C2 utilized in this study was 2.8 μmol of 1-acenaphthenol (1mM) oxidized/min/mg. Stereospecifically labeled (4-*pro*-*R*)-[4-^{2}H]NADPH (NADPD) was prepared enzymatically as previously described (25). Cofactors NADP(H) were obtained from Roche Diagnostics. All steroids were purchased from Steraloids. All other reagents were purchased from Sigma and are of ACS grade or better. Unless stated otherwise, all experiments were carried out at 25 ºC in 10 mM potassium phosphate buffer (pH 7.0) containing 1mM EDTA and 4% acetonitrile.

Steady-State Enzyme Kinetics

Initial rates of the NADPH dependent reduction of DHT catalyzed by AKR1C2 were measured with a Hitachi F-2500 fluorescence spectrophotometer by monitoring the change in fluorescence emission of NADPH. Excitation and emission wavelengths were set at 340 nm and 450 nm, respectively. Changes in fluorescence units were converted to nanomoles of cofactor by using standard curves of fluorescence emission versus known NADPH concentrations. Typical reaction samples contained 0.17 μM of AKR1C2, 12 μM of NADPH (saturating concentration) and DHT at varied concentrations (1.5 μM – 25 μM) in a total volume of 1 mL. Data were analyzed by nonlinear least-squares fitting to the equation,

$$\upsilon = k_{cat}[E][S]/(K_m + [S]) \quad (1)$$

where υ is the initial velocity, [E] and [S] are the total molar concentrations of the enzyme and steroid substrate, respectively, k_{cat} (s^{-1}) is the turnover number, and K_m (μM) is the apparent Michaelis-Menten constant for the steroid substrate.

Similarly, initial-rate measurements were carried out using NADPD as the cofactor in place of NADPH. Primary deuterium KIEs on apparent steady-state kinetic parameters for the reduction of DHT were obtained and reported using the nomenclature of Northrop (31), whereby $^D k_{cat}$ is the ratio of k_{cat} determined in the presence of NADPH relative to k_{cat} determined in the presence of NADPD, and $^D(k_{cat}/K_m)$ is the ratio of k_{cat}/K_m determined in the presence of NADPH relative to the k_{cat}/K_m determined in the presence of NADPD.

Equilibrium Ligand Binding

Apparent dissociation constants for enzyme-cofactor binary complexes were determined from fluorescence titration data. The quenching of intrinsic fluorescence of the free protein upon

binding of the cofactor was monitored using a Hitachi F-2500 fluorescence spectrophotometer set at an excitation wavelength of 290 nm and an emission wavelength of 340 nm. Each sample contained 0.20 μM of protein, to which small volumes of NADPH or $NADP^+$ (final concentrations 40 nM to 12 μM) were added incrementally. The total volume change from the addition of the cofactor was less than 2%.

Eq. 2a and 2b were used to fit the titration data.

$$\Delta F/\Delta F\ \max = [\mathrm{EC}]/[\mathrm{E}] \tag{2a}$$

$$[\mathrm{EC}]=\{(K_d+[\mathrm{E}]+[\mathrm{C}]) - [(K_\mathrm{d}+[\mathrm{E}]+[\mathrm{C}])^2 - 4[\mathrm{E}][\mathrm{C}]]^{1/2}\}/2 \tag{2b}$$

where ΔF is the difference in protein emission in the absence and presence of cofactor, ΔF_{max} is the maximum value of ΔF at saturating cofactor concentration, [EC] is the concentration of cofactor-bound enzyme, [E] is the total concentration of the enzyme, [C] is the total concentration of the added cofactor, and K_d is the apparent dissociation constant of the cofactor.

Transient Kinetics of Ligand Binding

All stopped flow experiments were performed on an Applied Photophysics SX-18MV stopped-flow spectrophotometer (Leatherhead, UK). The deadtime of the instrument was about 1.5 ms. Data were collected and analyzed using the Applied Photophysics software.

The quenching of the intrinsic fluorescence of AKR1C2 was monitored upon rapid mixing of equal volumes of the enzyme solution (AKR1C2, 1 or 2 μM) and the cofactor solution (NADPH 0–40 μM or $NADP^+$ 0–140 μM). The excitation wavelength was set to 285 nm and emission at 330 nm was monitored by the use of an interference filter. For each concentration of the cofactor, the data from at least five replicates were averaged and fitted to either single- (eq. 3) or double-exponential equations (eq. 4).

$$y=A\exp(-k_{\mathrm{obs}}\,t)+a \tag{3}$$

$$y=A_1\exp(-k_{\mathrm{obs1}}\,t)+A_2\exp(-k_{\mathrm{obs2}}\,t)+a \tag{4}$$

where y is the fluorescence signal, A, A_1, and A_2 are the amplitudes, *a* is the intercept, and k_{obs}, k_{obs1}, and k_{obs2} are the apparent rate constants.

Transient Kinetics of Substrate Turnover

For stopped-flow turnover experiments, the change in fluorescence signal of NADPH (excitation 340 nm, emission 450 nm) was monitored upon rapid mixing of equal volumes of the premixed enzyme-cofactor solution from one syringe and DHT from a second syringe.

For single turnover experiments, the enzyme-cofactor solution contained a fixed concentration of AKR1C2 (0.9 μM) and sub-stoichiometric concentration of NADPH (0.8 μM), and the substrate solution contained DHT at varied concentrations (0–45 μM). For each concentration of the steroid used, the averaged reaction traces from at least three replicates were fitted to either single- (eq. 3) or double-exponential functions (eq. 4). Secondary plots of the from the single-exponential analysis k_{obs} versus [S] displayed saturation kinetics and were fitted to the hyperbolic equation

$$k_{\mathrm{obs}}=k_{\mathrm{lim}}[\mathrm{S}]/(K_{1/2}+[\mathrm{S}]) \tag{5}$$

where $k_{trans} = k_{lim}$ is the limiting rate constant for the single turnover reactions and $K_{1/2}$ is the apparent half-saturation constant.

Similarly, single turnover experiments were carried out substituting NADPD for NADPH. The isotope effect on k_{trans} is obtained as $^{D}k_{trans}$, the ratio of k_{trans} in the presence of NADPH relative to that in the presence of NADPD.

For stopped-flow multiple turnover experiments, the enzyme solution contained a fixed concentration of AKR1C2 (1.7μM) and excess NADPH (20 μM), and the substrate solution contained DHT at concentrations in the range of 16–45 μM. For each concentration of the steroid used, the averaged reaction traces from at least three replicates were fitted to either the linear (eq. 6) or the "burst" equations (eq. 7) (32).

$$y = k_{obs} t + a \quad (6)$$

$$y = A \exp(-k_{obs1} t) + k_{obs2} t + a \quad (7)$$

where k_{obs} and k_{obs2} are the second–order rate constants of the linear steady-state phase, and k_{obs1} is the pseudo first-order rate constant of the exponential phase. Secondary plots of the k_{obs} values from the burst analysis versus [S] were fitted to the hyperbolic eq. 5, where $k_{burst} = k_{lim1}$ is the limiting rate constant for the burst phase and $k_{ss} = k_{lim2}/[E]$ is the limiting rate constant for the steady state linear phase.

Stopped-flow transient turnover experiments were also conducted in the absorption mode of the instrument by monitoring the changes in the absorbance signal of NADPH at 340nm. For single turnover reactions, the premixed enzyme-cofactor solution contained 3.2 μM AKR1C2 and 3.0 μM NADPH, and the steroid solution contained 50 μM DHT. For multiple turnover reactions, the premixed enzyme-cofactor solution contained 5.0 μM AKR1C2 and 130 μM NADPH, and the steroid solution contained 50 μM DHT.

Global Fitting and Simulations

Stopped-flow progress curves of cofactor binding and turnover reactions were globally analyzed using the program DynaFit (BioKin, Ltd., Pullman, WA) (33). Experimentally determined rate constants provided initial estimates for the fitting (details see Results). Actual concentrations were used and allowed to vary within 10%.

For the binding of the cofactor to AKR1C2, two models were considered as shown in Scheme 2 and 3, where k_1 and k_2 denotes the rate constants for the association and dissociation of the loose complex of NADP(H) to AKR1C2, k_3 and k_4 denote the isomerization of binary complexes in a two step model, and k_3, k_4, k_5, k_6 denote the isomerization processes in a three step model.

For single turnover experiments, catalytic sequences described in Scheme 4 were modeled, where the definitions of the rate constants follow Scheme 1. In addition, the non-enzymatic decay of the reduced cofactor was considered.

For multiple turnover experiments, the whole catalytic sequence described in Scheme 1 was modeled.

RESULTS

Steady State Kinetics and KIEs

The steady state NADPH dependent reduction of DHT catalyzed by AKR1C2 had a turnover number of 0.033 ± 0.002 s^{-1} at 25 °C pH 7.0. The apparent K_m for DHT was 2.9 ± 0.2 μM. Using NADPD as the cofactor, primary isotope effects were measured to be $^{D}k_{cat}$ of 1.5 ± 0.1 and $^{D}(k_{cat}/K_m)$ of 2.1 ± 0.1. For an ordered bi bi mechanism as shown in Scheme 1, the small magnitude of the primary KIEs in k_{cat} and k_{cat}/K_m suggests the chemical step is partially rate limiting and that product release step(s) are slow and can mask the true isotope effect on the hydride transfer step.

The enzyme also catalyzes the oxidation of Diol with a low k_{cat} of 0.008 ± 0.002 s^{-1} and the apparent K_m for Diol of 3.1 ± 0.2 μM. The oxidative reaction is unfavored in a cellular environment where NAD^+ would be the preferred cofactor (8). Previous studies had shown that the NAD^+-dependent oxidation of Diol is potently inhibited by the opposing cofactor NADPH (10). Further detailed kinetic characterization on the transient turnovers of Diol catalyzed by AKR1C2 were thus not pursued. To dissect the NADPH-dependent reduction of DHT catalyzed by AKR1C2, discrete steps were examined.

Kinetics of Cofactor Binding and Release

The quenching of the intrinsic protein fluorescence of AKR1C2 upon cofactor binding was utilized to measure the dissociation constants of the cofactors. AKR1C2 contains three tryptophans and in the crystal structure Trp86 is in close proximity to the nicotinamide ring of the cofactor. Trp86 is likely the residue quenched by cofactor binding as it was the case for the rat enzyme AKR1C9 (34). Fluorescence quenching yielded K_d values of 0.12 ± 0.02μM and 0.21 ± 0.03 μM for the binding of NADPH and $NADP^+$ to AKR1C2, respectively.

The quenching of the protein fluorescence was accompanied by kinetic transients that were observed by stopped flow measurements (Figure 2). Control experiments with tryptophan and cofactors showed no kinetic transient, confirming that kinetic transients observed upon mixing AKR1C2 with either NADPH or $NADP^+$ were AKR1C2 dependent. Similar kinetic transients were observed with $NADP^+$ and NADPH excluding the contribution of an inner filter effect. Transient traces were first analyzed by fitting to single-exponential (eq. 3) or double-exponential (eq. 4) equations. For both cofactor ligands, fitting to the double-exponential functions were superior, which yielded two observed rate constants (k_{obs}). Biphasic transient behaviors are consistent with kinetic binding mechanisms that comprise a fast binding step to form a loose complex followed by one or more isomerization steps to form the end tight complex. Schemes 2 and 3 describe the two- and three-step binding models, respectively. However, plots of the k_{obs} values from both the fast and the slow phases versus cofactor concentration displayed saturation kinetics, thus supporting the three-step binding model.

Progress curves of cofactor binding were globally fitted and simulated by using the program DynaFit. Several binding models, which included the 2-step model, 3-step model, and models with enzyme isomerization prior to cofactor binding, were tested and compared. The 3-step model described in Scheme 3 gave the best fitting results to the experimental data and was clearly favored by the model discrimination function of the program. Global analysis of the progress curves provided estimates for the microscopic rate constants of the steps. The rate constants for the first two steps in the 3-step binding model were not as well defined as k_5 and k_6 such that multiple sets of solutions for (k_1 and k_2, k_3 and k_4) generated similar fits. The values listed in Table 1 were chosen to simulate the experimental traces of cofactor binding (Figure 3) based on the following two considerations. (1) k_1 can not be higher than 1.0×10^9 M^{-1} s^{-1} (diffusion limit); and (2) k_3 should be in line with the maximum value of k_{obs1} (apparent

rate constant of the fast phase at saturating concentrations of the cofactor) from primary analysis. Solutions of k_3 that were orders of magnitude higher or lower were discarded.

The rate constants in Table 1 show that the cofactor binds to the enzyme to form a loose E•NADP(H) complex, which undergoes two subsequent conformational changes to yield a tight E**•NADP(H) complex, making the release of NADPH or $NADP^+$ a slow process. For the reaction in the reduction direction, the microscopic events for the release of $NADP^+$ would give an effective macroscopic rate constant (k_{Qr})[3] of 0.29 s^{-1}, which is less than 10-fold higher than the overall turnover rate in steady state. This suggested the release of the cofactor product $NADP^+$ during DHT reduction may be involved in rate determination, but cannot be the sole contributor.

Transient Single Turnover Reactions

To monitor the reduction of DHT under single turnover conditions, the enzyme was premixed with a sub-stoichiometric amount of the cofactor so that the enzyme could not recycle. DHT was then added from a second syringe. A representative stopped-flow trace of the fluorescence signal at 450 nm for the single turnover of DHT catalyzed by AKR1C2 is shown in Figure 4. The progress curves were fitted to a single exponential function (eq. 3).[4] Similar results were obtained when the reaction was followed in the absorption mode (340 nm). However, this required a high concentration of enzyme, which in turn necessitated the use of high concentrations of DHT to satisfy pseudo first-order conditions ([DHT] ≥ 8 [E]). As a consequence, the limit of DHT solubility[5] prevented the use of the absorbance mode over a wide range of DHT concentrations. Thus the fluorescence data obtained were used for further analysis and fitting. The observed pseudo-firstorder rate constants (k_{obs}) from fluorescence traces were plotted as a function of DHT concentration, which was fitted to the general hyperbola (eq. 5), yielding a k_{lim} value of 0.108 ± 0.004 s^{-1}. This k_{lim}, termed as k_{trans}, is the maximum first-order rate constant for single turnover at saturating DHT concentrations. Under this condition, the reaction sequence monitored included the binding of the steroid substrate, the chemical event, and the release of the steroid product. The magnitude of k_{trans} was only 4 fold greater than the k_{cat} determined by steady state methods, indicating that one or more of these events contributed to rate determination. When NADPH was substituted by NADPD, a k_{trans} value of 0.031 ± 0.001 s^{-1} was obtained, thus yielding an apparent $^D k_{trans}$ of 3.5. Since $^D k_{cat}$ in the steady state was smaller, i.e. 1.5, this difference further indicated that steps following the chemical event, i.e. product release steps, masked the isotopically sensitive hydride transfer step, resulting in a small $^D k_{cat}$ in the steady state.

The progress curves of the single turnover reaction were fitted to the model described in Scheme 4 using DynaFit. The fitting generated estimates for the rate constants of the DHT binding events (k_{Bb} and k_{Br}) and the chemical conversion (k_{red} and k_{oxi}). However, the result of the fitting was insensitive to the changes in the rate constant of the product release step (k_{Pr}). The average error for the rate constants was below 10 % except for k_{oxi} (~ 30 %). Consideration of the non-enzymatic decay of the cofactor improved the fitting modestly. Similarly, the data set for the single turnover reaction using NADPD as cofactor was fitted. Only the rate constants of the isotopic sensitive steps (i.e. k_{red} and k_{oxi}) varied significantly between the NADPH and NADPD data sets. Representative experimental and simulated progress curves of the single

[3] k_{Qr} was calculated with the equation $k_{Qr} = k_2\, k_4\, k_6/(k_2\, k_4 + k_2\, k_5 + k_3\, k_5)$.

[4] Some reaction traces can be fitted to double-exponential decay with similar or better residuals, which resulted in two observed rate constants that were 4–6 fold apart. Comparison of the slower rate constant with the rate constant determined in the absence of DHT indicated that the slow non-enzymatic decay of NADPH was not the source of the slow phase. Since it was difficult to discern between single- and double-exponential fittings, all traces were analyzed by fitting to a single-exponential decay.

[5] The solubility of DHT at 25 °C and pH 7.0 in 4 % methanol was estimated to be about 40 μM.

turnover reaction of DHT catalyzed by AKR1C2 are shown in Figure 5. The values of the rate constants used in simulation are listed in Table 2.

For the reduction of DHT, the hydride transfer step with NADPH as the cofactor occurred at 0.12 s^{-1}, while the corresponding event with NADPD took place at 0.039 s^{-1}. This yielded an intrinsic isotope effect of 3.1, which is in reasonable agreement with the apparent primary KIE of 3.5 seen under single turnover conditions.

Transient Multiple Turnover Reactions

In stopped-flow multiple turnover experiments, AKR1C2 was allowed to react with excess NADPH and DHT. The fluorescence time courses of the NADPH depletion were curvilinear and were best fitted to the "burst" equation of eq. 7, which is the sum of an exponential term and a linear term (Figure 6) (32). Fitting data to a linear regression, or single or double exponential functions were also attempted, but proved to be unsuitable based on the size of the residuals. Thus the transient state, multiple turnovers of DHT catalyzed by AKR1C2 occurred with an initial burst (exponential phase) corresponding to the first turnover during which NADPH decayed more rapidly, followed by a slower rate of product formation (linear phase) corresponding to steady state turnover. Similar results were obtained when the reaction was followed in the absorption mode (340 nm). As with single turnover reactions, it was not possible to monitor the reaction in the absorption mode over a range of DHT concentrations due to the limit of DHT solubility.

Fluorescence data were used for further analysis and fitting. It was difficult to obtain robust fits for both the exponential and linear phases of the reaction over a wide range of DHT concentrations, because of the small amplitude of the exponential phase and the short linear window for the steady-state turnover limited by substrate concentrations. Despite the limited data set and its relatively large errors, the observed rate constants for the exponential and linear phases at apparent saturation gave k_{burst} and k_{ss} values of 0.12 ± 0.03 s^{-1} and 0.032 ± 0.004 s^{-1}, respectively. These values were in agreement with the k_{trans} of 0.108 s^{-1} and the k_{cat} of 0.033 s^{-1} determined by transient single turnover and steady state turnover experiments, respectively. The observed "burst" in product formation indicated the presence of one or more slower steps following the chemical step. The fact that k_{burst} was only slightly greater than k_{ss} also suggested that these steps have comparable rates. As a result, the traces do not display a classic "burst" profile in which a significant burst is present. The amplitude of the burst phase, which corresponded to <0.30 enzyme equivalents, dictated that the differences in the rates of product formation and release must be small (32).

The fluorescence transients for the reduction of DHT under multiple turnover conditions catalyzed by AKR1C2 were fitted and simulated using DynaFit according to the minimal bi bi order mechanism described in Scheme 1. In the fitting trials, the rate constants determined from the single turnover data were used to estimate the remaining rate constants. Multiple pairs of k_{Ab} and k_{Ar} values (which govern the binding and release of NADPH, respectively) values gave similar fitting results, the pair chosen agreed most with those determined independently in the cofactor binding experiments. Unlike the fitting for the single turnover data, the fitting of the multiple turnover data was sensitive to the value of k_{Pr} (the release of Diol). It was found that the initial curvature in the progress curve could only be simulated if either one or both of the product release steps values (k_{Pr} and k_{Qr}, the release of $NADP^+$) were smaller than k_{red}. Simulated multiple turnover progress curves using rate constants listed in Table 2 are shown in Figure 7. The best simulation were obtained when hydride transfer from NADPH (k_{red}) occurred with a rate constant of approximately 0.12 s^{-1}, the release of the steroid product (k_{Pr}) occurred at a rate constant of 0.081 s^{-1}, and the release of $NADP^+$ (k_{Qr}) occurred at rate constant of 0.21 s^{-1}. Because the product formation and product release events occur at very

similar rates, all the above events were significant in determining the overall rate of catalysis, and hence the elimination of the androgen signal.

DISCUSSION

Human AKR1C enzymes via their 3-, 17-, and 20-ketosteroid reductase activities can regulate ligand access to the androgen, estrogen, and progestin receptors in target tissues (6). The importance of these reactions warrants detailed structural and kinetic information on these enzymes. We now report the dissection of the discrete steps involved in the elimination of the androgen signal catalyzed by AKR1C2.

In human prostate, the androgen signal is produced by the reduction of circulating testosterone to DHT catalyzed by the type 2 5α-reductase (5R2). It is then eliminated by the reduction of DHT to Diol catalyzed by AKR1C2. In this sequence, AKR1C2 catalyzes the rate determining step, since 5R2 has a V_{max} of 2 nmol/min/mg and a K_m for testosterone of ~ 0.5 μM (35), while AKR1C2 has a V_{max} of 0.82 nmol/min/mg and a K_m of ~3 μM for DHT. Recent estimates of 5R2 and AKR1C2 expression levels showed that mRNA levels of AKR1C2 were 2- and 10-fold higher than those of 5R2 in stromal and epithelial cells, respectively (Bauman and Penning, unpublished). The balance of kinetic properties and expression levels suggests that DHT synthesized by 5R2 can be efficiently eliminated by AKR1C2.

The apparent k_{cat} of AKR1C2 is related to the individual steps of the ordered bi bi mechanism described in Scheme 1 by eq. 8 (36).

$$k_{cat}=k_{red}k_{Pr}k_{Qr}/(k_{red}k_{Pr}+k_{red}k_{Qr}+k_{Pr}k_{Qr}+k_{oxi}k_{Qr}) \quad (8)$$

k_{cat} represents the slowest step if that step is dominating. This study shows that the rate determining events in DHT turnover catalyzed by AKR1C2 include the chemical step (k_{red} of 0.12 s^{-1}), steroid product release (k_{Pr} of 0.081 s^{-1}), and cofactor product release (k_{Qr} of 0.21 s^{-1}). Since these events have comparable rates, all contribute to k_{cat} significantly and there is no dominating slow step for AKR1C2 catalysis.

Using the estimated rate constants of individual steps, steady state kinetic parameters for the AKR1C2 catalyzed reduction of DHT and oxidation of Diol were calculated, which in general agreed with the measured values (Table 3). The calculated KIE values were consistent with experimental values, where a small normal $^{D}k_{cat}$ and a slightly larger $^{D}(k_{cat}/K_m)$ were obtained. The predicted low micromolar K_d values for DHT and Diol for AKR1C2 were also in agreement with the K_d values of steroids determined previously for AKR1C9.[6]

Kinetic behavior of AKR1C2 (in the NADPH-dependent reduction of DHT) can be compared with the behavior of its rat homolog AKR1C9 (in the same reaction) (25), and the more distant superfamily members AKR1B1 (in the NADPH-dependent reduction of xylose) (23) and AKR2B5 (in the NADH-dependent reduction of xylose) (24) (Table 4). This comparison shows that rate determination of AKR catalysis is enzyme dependent. While multiple steps govern the k_{cat} of AKR1C2 reaction, chemical conversion is a major rate-determining step for AKR1C9 and the cofactor release step largely controls the overall rates of the AKR1B1 and AKR1B2 catalyzed reactions.

A common theme in AKR catalysis is that the rate of cofactor release is strongly linked to rate-determination. Large differences in cofactor affinity have been noted among members of

[6]The formation of the AKR1C9•NADPH•steroid ternary complex is accompanied by the quenching of the energy-transfer band at 450 nm, which can be used to determine dissociation constants of steroids (37). Unlike the AKR1C9 system, the binding of NADPH to AKR1C2 does not result in an energy transfer band that can be further quenched by binding steroid (Jin and Penning, unpublished results).

different subfamilies, which range from low nM for AKR1B1 to low μM for AKR2B5 (23, 24). Despite these differences, transient kinetic studies of the cofactor binding processes show that significant conformational changes occur. Cofactor binding processes can occur in two steps for the binding of NADP(H) to AKR1B1 and for the binding of NAD(H) to AKR2B5, or three steps for the binding of NADP(H) to AKR1C2 and AKR1C9 (27). The isomerization steps result in the tightening of the initial loose binary complex by one to three orders of magnitude.

In the 3-step binding model of NADP(H) to AKR1C2, at least one of the isomerization steps reflects the anchoring of the 2′-phosphate group of AMP in NADP(H), since the binding of NAD(H) to AKR1C2 can be explained by a two-step model (Jin and Penning, unpublished result), similar to that observed for AKR2B5. k_{Qr} for $NADP^+$ from AKR1C2 was estimated to be 0.29 s^{-1} by stopped-flow cofactor binding experiments or 0.21 s^{-1} by transient turnover simulation. Although these values are almost 10 fold higher than k_{cat} (0.033 s^{-1}), k_{Qr} is comparable to the other two slow events in the catalytic sequence, which when combined determine the k_{cat} for AKR1C2 catalysis.

The binding of the cofactor to AKR1B1 is tight due to the formation of a “safety-belt” structure, which is absent in AKR1C2, AKR1C9, and AKR2B5 (13,14,38,39). The net rate constant for the release of the cofactor product $NADP^+$ (k_{Qr}) for AKR1B1 was reported to be 0.18 s^{-1}, essentially dominating the k_{cat} (0.19 s^{-1}) (Table 4) (23). Although occurring at a much faster rate, cofactor release was also proposed to be largely rate limiting for the xylose reduction catalyzed by AKR2B5 (24). k_{Qr} for NAD^+ from AKR2B5 is calculated to be 19.6 s^{-1} based on reported microscopic rate constants, which is less than 2 fold greater than its k_{cat} (12.4 s^{-1}).

In contrast to the slow release of cofactor which is characteristic of different AKRs, the rates of the chemical transformation and alcohol product release steps, and their contribution to rate determination can differ significantly. Carbonyl reduction (k_{red} in table 4) catalyzed by AKR1C2 occurs at a rate more than 1000-fold slower than that catalyzed by aldose and xylose reductases. Considering the high conservation in spatial arrangement of the active site of AKR enzymes revealed from crystal structures, it may appear contradictory for these enzymes to have vastly different rates of chemical conversion. However, the substrate binding pockets of the AKRs exhibit great variation in structure. Previous studies with AKR1C9 revealed that the rate of chemical conversion is very sensitive to perturbation in the structure of the steroid binding site (25,37). The AKR1C9 W227A mutant resulted in a 10-fold decrease in the maximal rate of single turnover (k_{trans}), which largely represents k_{red} for DHT reduction catalyzed by this enzyme. More strikingly, single Ala mutations of steroid contact residues in AKR1C9 resulted in decreases in k_{trans} for the oxidation of androsterone by several orders of magnitude. It is likely that for all AKR enzymes the positioning of the carbonyl substrate determined by the structure of the substrate binding pocket of the enzyme significantly affects the rate of the chemical conversion.

Structural differences in the substrate binding pockets of AKRs may also translate into major differences in the kinetics of carbonyl binding and alcohol release. Despite of the lack of a direct method to detect these events, the effect of k_{Pr} (rate of alcohol release) on k_{cat} in AKR1C2 catalysis was implicated. Transient kinetic studies of the cofactor binding process for AKR1C2 provided an estimate for the effective macroscopic rate constant of $NADP^+$ release (k_{Qr}) to be 0.29 s^{-1}. This k_{Qr} would not be able to account for the burst in product formation during multiple turnover which requires either k_{Pr} (the release of Diol) or $k_{Qr,}$ or both to be slower than k_{red} (0.12 s^{-1}). Thus k_{Pr} has to be slower than the chemical conversion (k_{red}). Kinetic simulation confirmed this conclusion by yielding a mechanism in which k_{Pr} was slightly slower than k_{red}, while k_{Qr} was 2-fold faster than k_{red}. Thus, the release of the steroid product was the

slowest (but not a dominating) step in the catalytic sequence. In contrast, k_{Pr} was estimated to be very fast for the reactions catalyzed by AKR1B1 and AKR2B5 (23,24), being 6 and 3 orders of magnitude greater than their respective k_{cat} values. Therefore, k_{Pr} does not contribute to overall rate determination in AKR1B1 and AKR2B5.

The occurrence of conformational changes during steroid binding and release with AKR1Cs is indicated by the comparison of the binary and ternary structures of AKR1C9, which showed different conformations for portions of the loops involved in substrate binding (40,41). Furthermore, crystallographic and molecular docking data have shown that steroids can bind in alternative modes in AKR1C2 (14,15,42). Thus, the catalytic cycle of AKR1C2 catalysis may be stalled by one or more energy barriers related to these alternative binding modes for steroid.

In conclusion, we used KIEs and transient kinetics to study the reduction of DHT catalyzed by AKR1C2. This important reaction leads to the elimination of androgen signal in steroid target tissues. Our results point to a kinetic mechanism that comprises multiple slow steps with comparable rate constants, including the chemical step, the release of the steroid and cofactor products. Judging from the similar low k_{cat} values of other human steroid transforming AKR1C enzymes, it is predicted that a similar kinetic behavior may apply to these enzymes and their pre-receptor regulation of steroid hormone action.

Acknowledgements

The authors thank Drs. Vladi Heredia and William Cooper for the synthesis of NADPD.

Supported by NIH grant DK47015 to T.M.P.

References

1. Penning TM, Jin Y, Steckelbroeck S, Rizner TL, Lewis M. Structure-function of human 3α-hydroxysteroid dehydrogenases: genes and proteins. Mol Cell Endocrinol 2004;215:63–72. [PubMed: 15026176]
2. Jez JM, Flynn TG, Penning TM. A new nomenclature for the aldo-keto reductase superfamily. Biochem Pharmacol 1997;54:639–647. [PubMed: 9310340]
3. Hyndman D, Bauman DR, Heredia VV, Penning TM. The aldo-keto reductase superfamily homepage. Chem Biol Interact 2003;143-144:621–631. [PubMed: 12604248]
4. Penning TM. Molecular endocrinology of hydroxysteroid dehydrogenases. Endocrine Reviews 1997;18:281–305. [PubMed: 9183566]
5. Penning TM. Hydroxysteroid dehydrogenases and pre-receptor regulation of steroid hormone action. Hum Reprod Update 2003;9:193–205. [PubMed: 12861966]
6. Bauman DR, Steckelbroeck S, Penning TM. The roles of aldo-keto reductases in steroid hormone action. Drug News Perspect 2004;17:563–578. [PubMed: 15645014]
7. Penning TM, Burczynski ME, Jez JM, Hung CF, Lin HK, Ma H, Moore M, Palackal N, Ratnam K. Human 3α-hydroxysteroid dehydrogenase isoforms (AKR1C1-AKR1C4) of the aldo-keto reductase superfamily: functional plasticity and tissue distribution reveals roles in the inactivation and formation of male and female sex hormones. Biochem J 2000;351:67–77. [PubMed: 10998348]
8. Rizner TL, Lin HK, Peehl DM, Steckelbroeck S, Bauman DR, Penning TM. Human type 3 3α-hydroxysteroid dehydrogenase (aldo-keto reductase 1C2) and androgen metabolism in prostate cells. Endocrinology 2003;144:2922–2932. [PubMed: 12810547]
9. Penning TM, Steckelbroeck S, Bauman DR, Miller MW, Jin Y, Peehl DM, Fung KM, Lin HK. Aldo-keto reductase (AKR) 1C3: role in prostate disease and the development of specific inhibitors. Mol Cell Endocrinol 2006;316:1300–1309.
10. Steckelbroeck S, Jin Y, Gopishetty S, Oyesanmi B, Penning TM. Human cytosolic 3α-hydroxysteroid dehydrogenases (3α-HSDs) of the aldo-keto reductase (AKR) superfamily display significant 3β-

hydroxysteroid dehydrogenase (3β-HSD) activity: implications for steroid hormone metabolism and activation. J Biol Chem 2003;279:10784–10795. [PubMed: 14672942]

11. Davies P, Eaton CL. Regulation of prostate growth. J Endocrinol 1991;131:5–17. [PubMed: 1744559]
12. Wilson, JD. Androgens. In: Hardman, JF.; Limbird, LE., editors. Goodman & Gilman's Pharmacological Basis of Therapeutics. New York: 1996. p. 1441-1457.
13. Bennett, MJ.; Albert, RH.; Jez, JM.; Ma, H.; Penning, TM.; Lewis, M. Structure. 5. 1997. Steroid recognition and regulation of hormone action: crystal structure of testosterone and $NADP^+$ bound to 3α-hydroxysteroid/dihydrodiol dehydrogenase; p. 799-812.
14. Jin Y, Stayrook SE, Albert RH, Palackal NT, Penning TM, Lewis M. Crystal structure of human type III 3α-hydroxysteroid dehydrogenase/bile acid binding protein complexed with $NADP^+$ and ursodeoxycholate. Biochemistry 2001;40:10161–10168. [PubMed: 11513593]
15. Nahoum V, Gangloff A, Legrand P, Zhu DW, Cantin L, Zhorov BS, Luu-The V, Labrie F, Breton R, Lin SX. Structure of the human 3α-hydroxysteroid dehydrogenase type 3 in complex with testosterone and $NADP^+$ at 1.25-Å resolution. J Biol Chem 2001;276:42091–8. [PubMed: 11514561]
16. Couture JF, Legrand P, Cantin L, Luu-The V, Labrie F, Breton R. Human 20α-hydroxysteroid dehydrogenase: crystallographic and site-directed mutagenesis studies lead to the identification of an alternative binding site for C21-steroids. J Mol Biol 2003;331:593–604. [PubMed: 12899831]
17. Komoto J, Yamada T, Watanabe K, Takusagawa F. Crystal structure of human prostaglandin F synthase (AKR1C3). Biochemistry 2004;43:2188–2198. [PubMed: 14979715]
18. Jez JM, Bennett MJ, Schlegel BP, Lewis M, Penning TM. Comparative anatomy of the aldo-keto reductase superfamily. Biochem J 1997;326:625–636. [PubMed: 9307009]
19. Trauger JW, Jiang A, Stearns BA, LoGrasso PV. Kinetics of allopregnanolone formation catalyzed by human 3α-hydroxysteroid dehydrogenase type III (AKR1C2). Biochemistry 2002;41:13451–9. [PubMed: 12416991]
20. Askonas LJ, Ricigliano JW, Penning TM. The kinetic mechanism catalysed by homogeneous rat liver 3α-hydroxysteroid dehydrogenase: evidence for binary and ternary dead-end complexes containing non-steroidal anti-inflammatory drugs. Biochem J 1991;278:835–841. [PubMed: 1898369]
21. Ehrig T, Bohren KM, Prendergast FG, Gabbay KH. Mechanism of aldose reductase inhibition: binding of $NADP^+$/NADPH and alrestatin-like inhibitors. Biochemistry 1994;33:7157–7165. [PubMed: 8003482]
22. Neuhauser W, Haltrich D, Kulbe KD, Nidetzky B. NAD(P)H-dependent aldose reductase from the xylose-assimilating yeast *Candida tenuis*: isolation, characterization and biochemical properties of the enzyme. Biochem J 1997;326:683–92. [PubMed: 9307017]
23. Grimshaw CE, Bohren KM, Lai C-J, Gabbay KH. Human aldose reductase: rate constants for a mechanism including interconversion of ternary complexes by recombinant wild-type enzyme. Biochemistry 1995;34:14323–14330. [PubMed: 7578036]
24. Nidetzky B, Klimacek M, Mayr P. Transient-state and steady-state kinetic studies of the mechanism of NADH-dependent aldehyde reduction catalyzed by xylose reductase from the yeast *Candida tenuis*. Biochemistry 2001;40:10371–10381. [PubMed: 11513616]
25. Heredia VV, Penning TM. Dissection of the physiological interconversion of 5α-DHT and 3α-diol by rat 3α-HSD via transient kinetics shows that the chemical step is rate-determining: effect of mutating cofactor and substrate-binding pocket residues on catalysis. Biochemistry 2004;43:12028–12037. [PubMed: 15379543]
26. Penning TM, Jin Y, Heredia VV, Lewis M. Structure-function relationships in 3α-hydroxysteroid dehydrogenases: a comparison of the rat and human isoforms. J Steroid Biochem & Mol Biol 2003;85:247–255. [PubMed: 12943710]
27. Jin Y, Cooper WC, Penning TM. Examination of the differences in structure-function of human and rat 3α-hydroxysteroid dehydrogenase. Chem Biol Interact 2003;2003:143, 383–92.
28. Ratnam K, Ma H, Penning TM. The arginine 276 anchor for NADP(H) dictates fluorescence kinetic transients in 3α-hydroxysteroid dehydrogenase, a representative aldo-keto reductase. Biochemistry 1999;38:7856–7864. [PubMed: 10387026]
29. Burczynski ME, Harvey RG, Penning TM. Expression and characterization of four recombinant human dihydrodiol dehydrogenase isoforms: oxidation of trans-7, 8-dihydroxy-7,8-dihydrobenzo

[*a*]pyrene to the activated *o*-quinone metabolite benzo[*a*]pyrene-7,8-dione. Biochemistry 1998;37:6781–6790. [PubMed: 9578563]

30. Bradford MM. A rapid and sensitive method for the quantitation of microgram quantities of protein utilizing the principle of protein-dye binding. Anal Biochem 1976;72:248–254. [PubMed: 942051]
31. Northrop DB. Deuterium and tritium kinetic isotope effects on initial rates. Methods Enzymol 1982;87:607–625. [PubMed: 7176927]
32. Johnson KA. Transient-state kinetic analysis of enzyme reaction pathways. Methods Enzymol 1992;134:677–705. [PubMed: 2950300]
33. Kuzmic P. Program DynaFit for the Analysis of Enzyme Kinetic Data: application to HIV Proteinase. Anal Biochem 1996;237:260–273. [PubMed: 8660575]
34. Jez JM, Schlegel BP, Penning TM. Characterization of the substrate binding site in rat liver 3α-hydroxysteroid/dihydrodiol dehydrogenase: the roles of tryptophans in ligand binding and protein fluorescence. J Biol Chem 1996;271:30190–20198. [PubMed: 8939970]
35. Makridakis N, Akalu A, Reichardt JKV. Identification and characterization of somatic steroid 5α-reductase (SRD5A2) mutations in human prostate cancer tissues. Oncogene 2004;23:7399–7405. [PubMed: 15326487]
36. Segal, IH. Enzyme Kinetics. John Wiley and Sons; New York: 1975. p. 560-564.
37. Heredia VV, Cooper WC, Kruger RG, Jin Y, Penning TM. Alanine scanning mutagenesis of the testosterone binding site of rat 3α-hydroxysteroid dehydrogenase demonstrates contact residues influence the rate-determining step. Biochemistry 2004;43:5832–5841. [PubMed: 15134457]
38. Wilson DK, Nakano T, Petrash JM, Gabbay KH, Quiocho FA. An unlikely sugar substrate site in the 1.65 Å structure of the human aldose reductase holoenzyme implicated in diabetic complications. Science 1992;257:81–84. [PubMed: 1621098]
39. Kavanagh KL, Klimacek M, Nidetzky B, Wilson DK. Structure of xylose reductase bound to NAD $^{+}$ and the basis for single and dual co-substrate specificity in family 2 aldo-keto reductases. Biochem J 2003;373:319–26. [PubMed: 12733986]
40. Hoog SS, Pawlowski JE, Alzari PM, Penning TM, Lewis M. Three-dimensional structure of rat liver 3α-hydroxysteroid/dihydrodiol dehydrogenase: a member of the aldo-keto reductase superfamily. Proc Natl Acad Sci USA 1994;91:2517–2521. [PubMed: 8146147]
41. Bennett MJ, Schlegel BP, Jez JM, Penning TM, Lewis M. Structure of 3α-hydroxysteroid/dihydrodiol dehydrogenase complexed with NADP^{+} Biochemistry 1996;35:10702–10711. [PubMed: 8718859]
42. Jin Y, Penning TM. Molecular docking simulations of steroid substrates into human cytosolic hydroxysteroid dehydrogenases (AKR1C1 and AKR1C2): insights into positional and stereochemical preferences. Steroids 2006;71:380–391. [PubMed: 16455123]

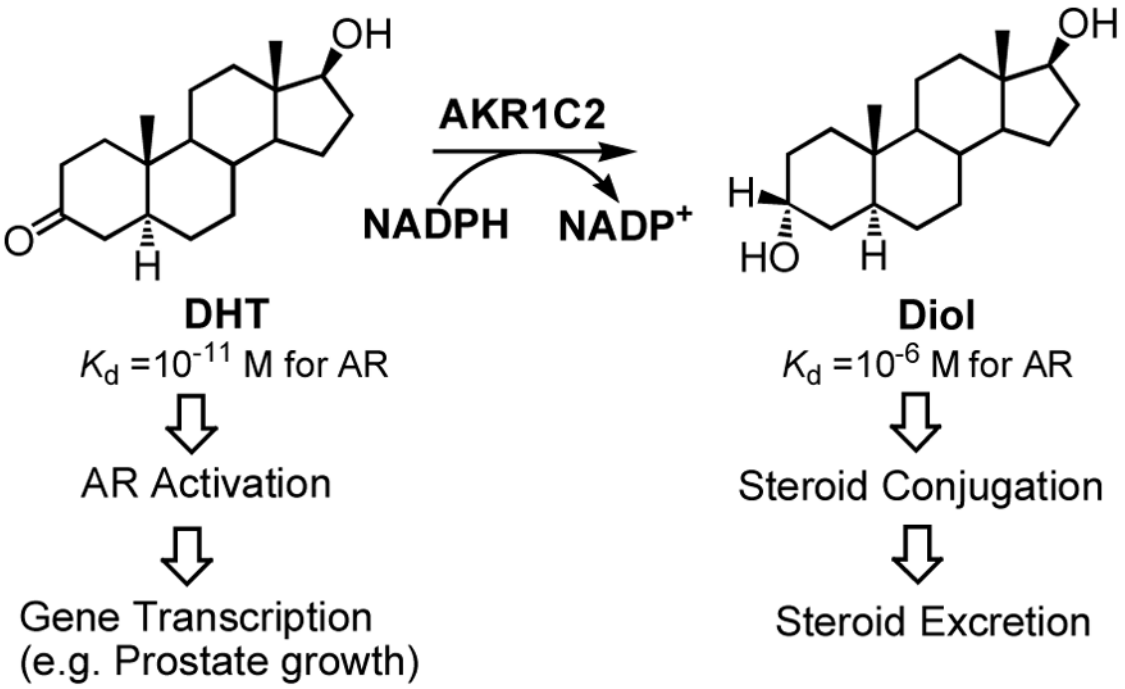

Figure 1.
Elimination of androgen signal by AKR1C2. AR= androgen receptor.

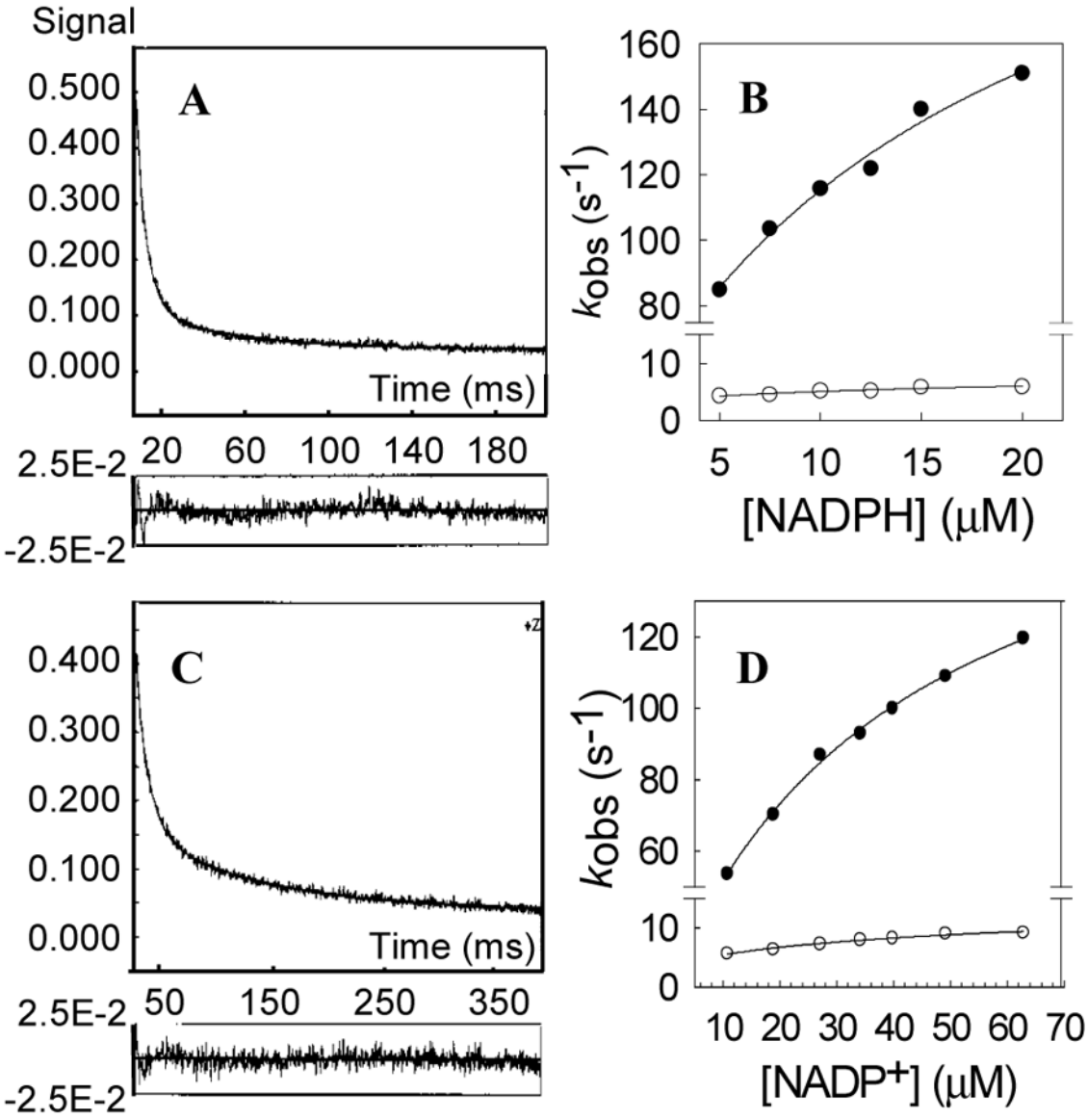

Figure 2.

Representative kinetic traces for the binding of NADPH and $NADP^+$ to AKR1C2. (A) The averaged progress curve for the quenching of protein fluorescence observed upon rapid mixing of the enzyme solution with the NADPH solution. The sample contained 0.5 μM AKR1C2 and 12.5 μM NADPH. Data were fitted to a double-exponential function (eq. 3), yielding A_1 = 0.55 ± 0.004 (Fluorescence unit), k_1 = 120 ± 1 (s^{-1}), A_2 = 0.16 ± 0.002 (Fluorescence unit), k_2= 7.7 ± 0.2 (s^{-1}). (B) Secondary plots of the observed rate constants versus [NADPH] fitted to a hyperbolic function. (C) The averaged progress curve for the quenching of protein fluorescence observed upon rapid mixing of the enzyme solution with the $NADP^+$ solution. The sample contained 1 μM AKR1C2 and 18.8 μM $NADP^+$. Data were fitted to a double-exponential function (eq. 3), yielding A_1 = 0.25 ± 0.002 (Fluorescence unit), k_1 = 90 ± 1 (s^{-1}), A_2 = 0.11 ± 0.001 (Fluorescence unit), k_2= 6.3 ± 0.2 (s^{-1}). (D) Secondary plots of the observed rate constants k_{obs1} (●) and k_{obs2} (○) versus [$NADP^+$] fitted to hyperbolic function.

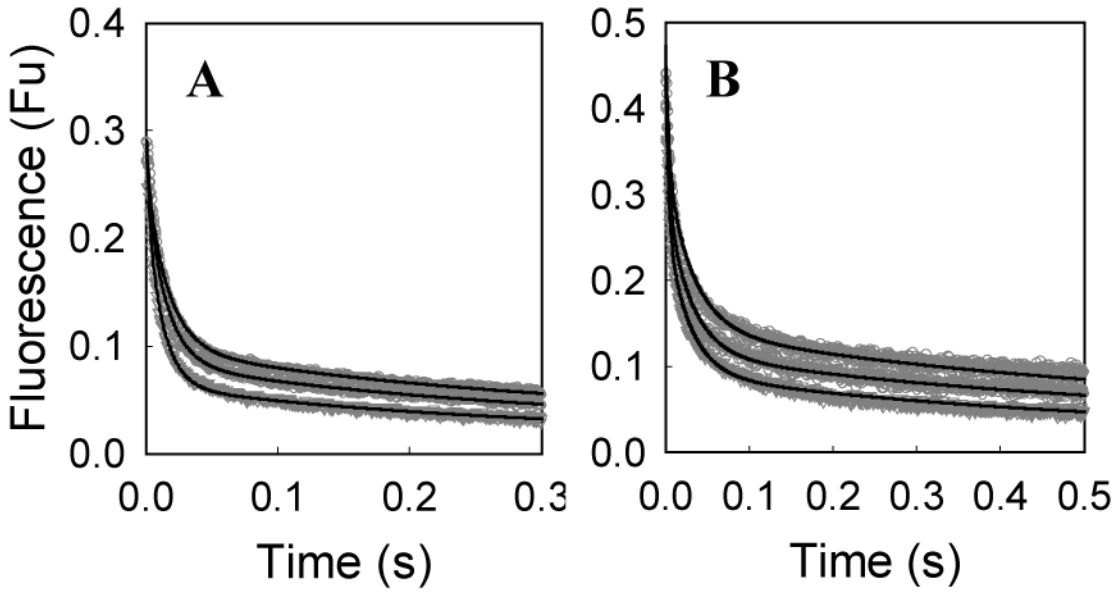

Figure 3.

Global simulation of progress curves for the binding of (A) NADPH and (B) $NADP^+$ to AKR1C2. Experimental (gray) and simulated (black) progress curves of protein fluorescence at 330 nm are shown. The samples contained 0.5 μM AKR1C2 and 5.0, 7.5, and 12.5 μM of NADPH (top to bottom in A) or 1 μM AKR1C2 and 10.8, 18.8, and 27.1 μM of $NADP^+$ (top to bottom in B) (all final concentrations). For clarity, data for other concentrations of cofactors were not shown, but were used in the global fitting. Simulated lines used microscopic rate constants from Table 1, fitted to the 3-step binding mechanism in Scheme 3.

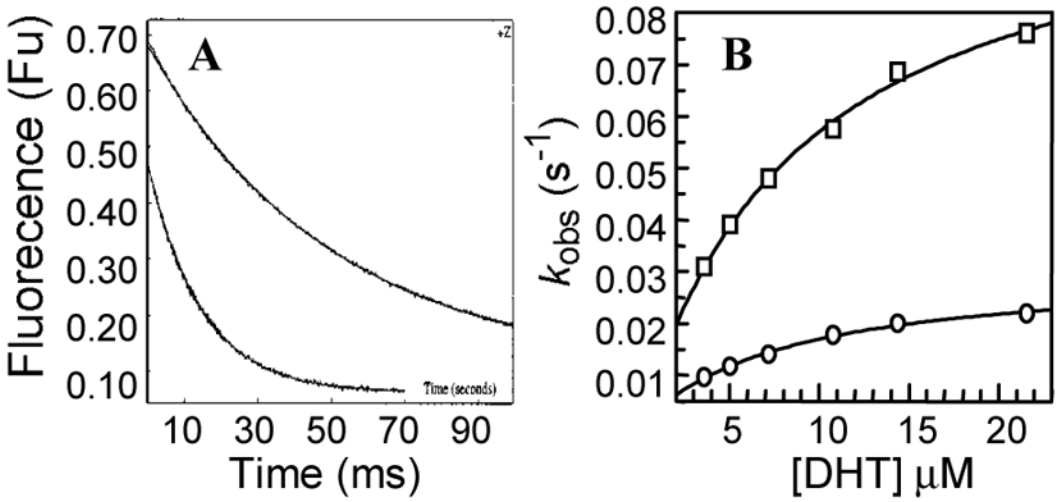

Figure 4.

Representative kinetic traces for the single turnover of DHT catalyzed by AKR1C2 using either NADPH or NADPD as cofactor. (A) The averaged progress curves for the reaction of the premixed enzyme-cofactor solution with DHT solution. The samples contained 0.45 μM AKR1C2, 0.4 μM NADPH (bottom trace) or 0.4 μM NADPD (top trace), and 10 μM DHT. Data were fitted to the single-exponential function (eq. 3). (B) Secondary plots of the apparent first-order rate constants k_{obs} for NADPH (□) or NADPD (○) versus [DHT], fitted to hyperbolic functions (eq. 5).

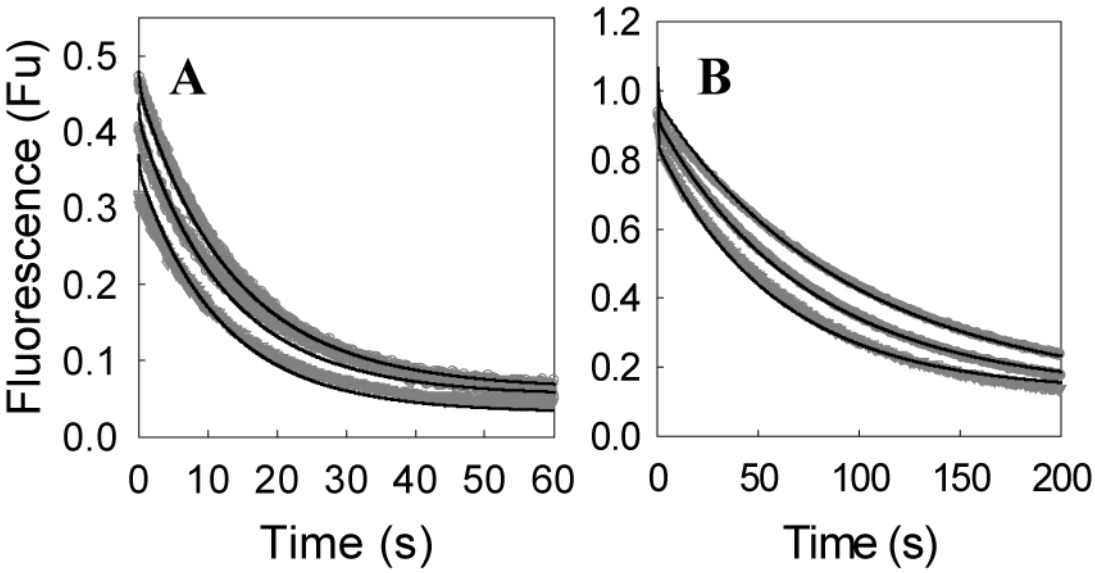

Figure 5.
Global simulation of progress curves for NADPH (A) and NADPD (B) dependent single turnover of DHT catalyzed by AKR1C2. Experimental (gray) and simulated (black) progress curves of decrease in NADPH fluorescence at 450 nm are shown. The samples contained 0.45 μM AKR1C2, 0.4 μM of NADPH or NADPD, and 5, 15, and 20 μM of DHT (traces top to bottom). For clarity, data for other concentrations of DHT were not shown, but were used in the global fitting. The simulated lines used rate constants from Table 2, fitted to the mechanism of Scheme 4.

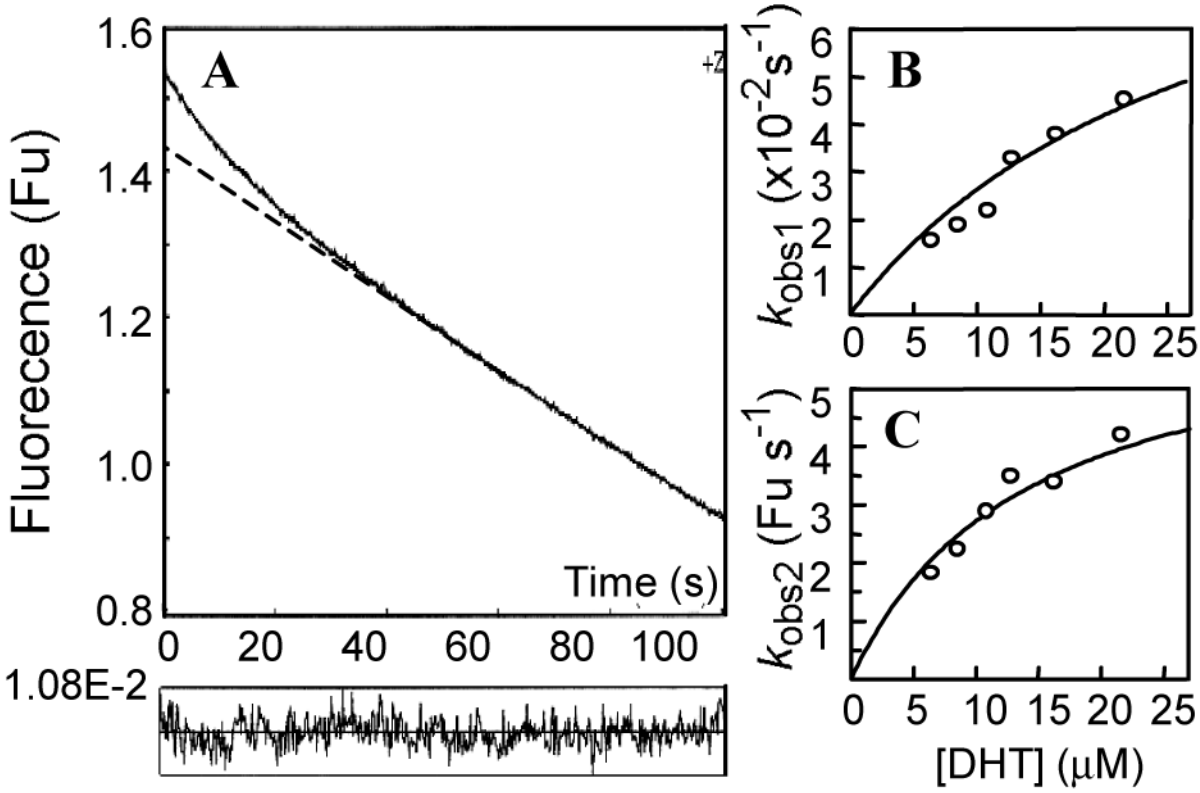

Figure 6.

Representative kinetic traces for the multiple turnover of DHT catalyzed by AKR1C2 in the transient state. (A) The averaged progress curve of NADPH fluorescence at 450 nm for the sample containing 0.85 μM AKR1C2, 10 μM NADPH, and 20 μM DHT. The trace was fitted to the burst equation (eq. 7), yielding the burst amplitude A_1 = 0.11 (Fluorescence unit), corresponds to 0.25 enzyme equivalents, k_{obs1} = 0.079 (s^{-1}), and k_{obs2}= 0.014 (μM s^{-1}). (B) and (C) Secondary plots of the observed rate constants k_{obs1} and k_{obs2} versus [DHT], fitted to a hyperbolic equation to yield k_{burst} and k_{ss}.

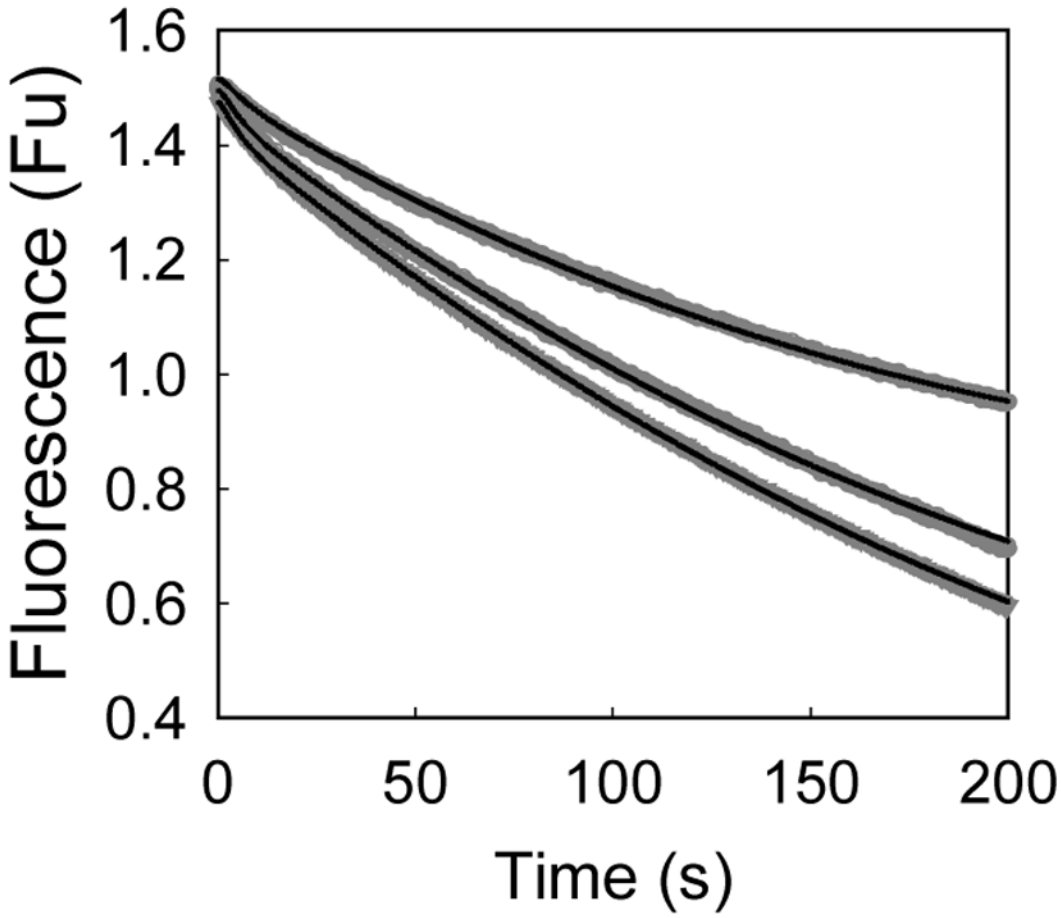

Figure 7.
Global simulation of progress curves for multiple turnover of DHT catalyzed by AKR1C2 in the transient state. Experimental (gray) and simulated (black) progress curves of NADPH fluorescence at 450 nm are shown. The samples contained 0.85 μM AKR1C2, 10 μM of NADPH, and 10, 15, and 20 μM of DHT (traces top to bottom). For clarity, data for other concentrations of DHT were not shown, but were used in the global fitting. The simulated lines used rate constants from Table 2, fitted to the mechanism of Scheme 1.

$$E + A \underset{k_{Ar}}{\overset{k_{Ab}}{\rightleftharpoons}} EA + B \underset{k_{Br}}{\overset{k_{Bb}}{\rightleftharpoons}} EAB \underset{k_{oxi}}{\overset{k_{red}}{\rightleftharpoons}} EPQ \underset{k_{Pb}}{\overset{k_{Pr}}{\rightleftharpoons}} EQ + P \underset{k_{Qb}}{\overset{k_{Qr}}{\rightleftharpoons}} E + Q$$

E = AKR1C2, A= NADPH, B = DHT, P = Diol, Q = $NADP^+$

Scheme 1.

$$\mathrm{E} + \mathrm{C} \underset{k_2}{\overset{k_1}{\rightleftharpoons}} \mathrm{EC} \underset{k_4}{\overset{k_3}{\rightleftharpoons}} \mathrm{E^*C}$$

$$\mathrm{C} = \mathrm{NADPH \text{ or } NADP^+}$$

Scheme 2.

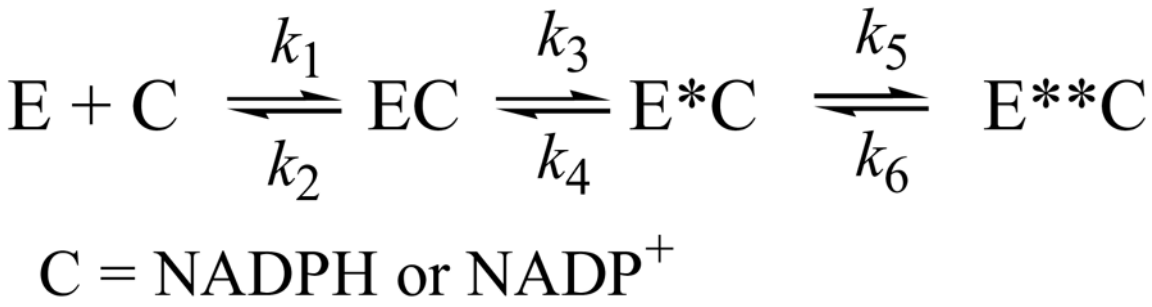

Scheme 3.

$$\mathrm{EA} + \mathrm{B} \underset{k_{\mathrm{Br}}}{\overset{k_{\mathrm{Bb}}}{\rightleftharpoons}} \mathrm{EAB} \underset{k_{\mathrm{oxi}}}{\overset{k_{\mathrm{red}}}{\rightleftharpoons}} \mathrm{EPQ} \underset{k_{\mathrm{Pb}}}{\overset{k_{\mathrm{Pr}}}{\rightleftharpoons}} \mathrm{EQ} + \mathrm{P}$$

Scheme 4.

Table 1

Rate constants used to simulate transient traces for cofactor binding to AKR1C2.

	NADPH	$NADP^+$
k_1 (μM^{-1} s^{-1})	21 ± 3	3.6 ± 0.1
k_2 (s^{-1})	200 ± 16	160 ± 10
k_3 (s^{-1})	150 ± 9	88 ± 6
k_4 (s^{-1})	44 ± 3	17 ± 2
k_5 (s^{-1})	3.5 ± 0.3	6.0 ± 0.5
k_6 (s^{-1})	1.8 ± 0.1	0.66 ± 0.04

Table 2

Rate constants used to simulate transient traces for single and multiple turnover of DHT catalyzed by AKR1C2.

Rate constants	Values
k_{Ab} (M^{-1} s^{-1})	(7.1 ± 0.1) ×10^6
k_{Ar} (s^{-1})	0.93 ± 0.07
k_{Bb} (M^{-1} s^{-1})[a]	(2.5 ± 0.4) ×10^5
k_{Br} (s^{-1})[a]	2.2 ± 0.2
k_{red} (s^{-1})[a]	0.12 ± 0.01 (0.039 ± 0.008)[b]
k_{oxi} (s^{-1})[a]	0.01 ± 0.003 (0.004± 0.001)[b]
k_{Pr} (s^{-1})[a]	0.081 ± 0.01
k_{Pb} (M^{-1} s^{-1})	(3.0 ± 0.8) ×10^4
k_{Qr} (s^{-1})	0.21 ± 0.03
k_{Qb} (M^{-1} s^{-1})	(2.1 ± 0.5) ×10^5

[a] Rate constants used to simulate the transient traces of single turnover reaction.

[b] Rate constants in brackets obtained from fitting the transient traces of single turnover reaction with NADPD.

Table 3

Comparison of rate constants determined from steady-state and pre-steady state studies.

	Measured	Calculated
k_{cat} (reduction) (s^{-1})	0.033 ± 0.002	0.039[a]
K_m (DHT) (μM)	2.9 ± 0.2	3.3[b]
$^{D}k_{cat}$	1.5 ± 0.1	1.7[c]
$^{D}(k_{cat}/K_m)$	2.1 ± 0.1	2.8[c]
k_{cat} (oxidation) (s^{-1})	0.008 ± 0.002	0.009[d]
K_m (Diol) (μM)	3.1 ± 0.2	3.0[e]
K_d (NADPH) (μM)	0.12 ± 0.02	0.21[f]
K_d ($NADP^+$) (μM)	0.21 ± 0.03	0.19[f]
K_d (DHT) (μM)	na	8.8[f]
K_d (Diol) (μM)	na	2.7[f]

[a] k_{cat} was calculated with eq. 8.

[b] K_m of DHT was calculated with the equation $K_m = k_{Qr}\,(k_{Br}\,k_{Pr} + k_{Br}\,k_{oxi} + k_{Pr}\,k_{red})/(k_{Bb}\,(k_{red}\,k_{Pr} + k_{red}\,k_{Qr} + k_{Pr}\,k_{Qr} + k_{oxi}\,k_{Qr}))$.

[c] $^{D}k_{cat}$ and $^{D}(k_{cat}/K_m)$ was calculated based on calculated k_{cat} and K_m values for NADPH and NADPD using corresponding rate constants listed in Table 2.

[d] k_{cat} for the oxidation direction was calculated with the equation $k_{cat}(\text{oxidation}) = k_{Ar}\,k_{Br}\,k_{oxi}/(k_{Ar}\,k_{Br} + k_{Ar}\,k_{red} + k_{Ar}\,k_{oxi} + k_{Br}\,k_{oxi})$.

[e] K_m of Diol was calculated with the equation $K_m = k_{Ar}\,(k_{Br}\,k_{Pr} + k_{Br}\,k_{oxi} + k_{Pr}\,k_{red})/(k_{Pb}\,(k_{Ar}\,k_{Br} + k_{Ar}\,k_{red} + k_{Ar}\,k_{oxi} + k_{Br}\,k_{oxi}))$

[f] K_d was calculated as the ratio of the release rate constant over the binding rate constant, i.e. K_d (NADPH) = k_{Ar}/k_{Ab}, K_d ($NADP^+$) = k_{Qr}/k_{Qb}, K_d (DHT) = k_{Br}/k_{Bb}, K_d (Diol) = k_{Pr}/k_{Pb}. na, not available.

Table 4

Comparison of the Rate Determining Events for AKR1C2, AKR1C9, AKR1B1, AKR2B5.

Enzyme	**AKR1C2**	**AKR1C9**[a]	**AKR1B1**[d]	**AKR2B5**[e]
Substrate	DHT	DHT	Xylose	Xylose
Cofactor	NADPH	NADPH	NADPH	NADH
k_{cat} (s^{-1})	0.033	0.30	0.19	14.2
K_m (μM)	2.9	0.7	1×10^3	7.8×10^4
k_{cat}/K_m (M^{-1} s^{-1})	9.3×10^3	4.3×10^5	190	140
$^{D}k_{cat}$	1.5	2.3[b]	1.00	1.55
$^{D}(k_{cat}/K_m)$	2.1	3.0[b]	1.82	2.09
k_{trans} (s^{-1})	0.11	1.9[c]	76	na
$^{D}k_{trans}$	3.5	Na	3.6	na
k_{red} (s^{-1})	0.12	Na	130	170
k_{Pr} (s^{-1})	0.081	Na	1×10^6	1×10^5
k_{Qr} (s^{-1})	0.21	Na	0.18	19.6[f]

[a] Rate constants as reported (25).

[b] These values are the averages of the previously reported and more recent measurements (Cooper and Penning., unpublished results).

[c] This value is from more recent measurements.

[d] Rate constants as reported (23).

[e] Rate constants as reported (24).

[f] This k_{Qr} value is calculated based on the reported (24) microscopic rate constants. na, not available.